

Eigenmode super-resolution imaging in arbitrary optical systems

Allan S. Johnson^{a*}, Kevin Piché^a, Jeff Z. Salvail^a, Jonathan Leach^{a†} and Robert W. Boyd^{a,b}

^aDepartment of Physics, University of Ottawa, Ottawa, Ontario, Canada; ^bInstitute of Optics, University of Rochester, Rochester, New York, 14627, USA

(Received 7 July 2013; accepted 28 October 2013)

We investigate optical super-resolution by means of eigenmode decomposition in arbitrary imaging systems. This technique is applicable for arbitrary objects but requires a knowledge of the eigenmodes of the imaging system. We outline a reconstruction technique that can be applied even to systems in which the eigenmodes are not orthogonal, and we present numerical simulations of eigenmode super-resolution in systems with resolution limited both by diffraction and by aberrations. Our results indicate that optical super-resolution by direct eigenmode decomposition provides a versatile method of sub-diffraction and distortion-free imaging in arbitrary optical systems.

Keywords: imaging and image processing; super-resolution; eigenmodes; image reconstruction

1. Introduction

Imaging is one of the most basic and fundamental tools in science, having nearly countless applications across chemistry, biology, physics and engineering. While the limit to imaging resolution was originally considered the Abbe diffraction limit [1], it is now well known that sub-diffraction imaging is possible. Super-resolution techniques, a blanket term for all imaging methods capable of overcoming the diffraction limit, have been of great interest ever since being first introduced in the 1960s [2,3]. Various super-resolution techniques have since been introduced, such as near field imaging with hyperlenses [4–7], non-linear fluorescence imaging [8–10], super-oscillatory lenses [11], compressive sensing [12,13], and quantum imaging protocols [14,15]. In practical terms, however, super-resolution techniques are quite limited. It would be advantageous to be able to super-resolve arbitrary samples without complex apparatus, in the presence of real world conditions such as turbulence, imperfect optics and diffraction.

Optical eigenmodes [16–19] provide a method to realize super-resolution without non-linear optical techniques or specialized imaging systems. Furthermore, eigenmodes provide an inherently robust technique, capable of imaging through aberrations and diffraction. If the eigenmodes of a system are known, images transmitted through the system can be decomposed into their component eigenmodes. By compensating for the attenuation and phase shift of the individual modes, a super-resolved image can be reconstructed. This form of eigenmode imaging, and its extension

to singular value decomposition, was originally considered infeasible due to computational costs and lack of a means for determining the eigenmodes of a system [20]. Further developments have thus focused on indirect methods, especially scanning microscopy [21] and the use of pupil-plane masks [22].

Recently we have experimentally demonstrated the feasibility of eigenmode super-resolution imaging in the special case where the eigenmodes are known analytically [23]. Here, we show how to determine the eigenmodes of an arbitrary optical system using the same technology, and utilize them for sub-diffraction and aberration tolerant imaging. We demonstrate the technique in diffraction-limited and aberrated systems with numerical simulations and show the viability of direct decomposition in modern imaging. We refer to this technique as eigenmode super-resolution imaging as it provides an increase in resolution, whether applied to sub-diffraction or aberration-free imaging. Optical eigenmodes also enable experimental examination of the ultimate limits to resolution imposed by the quantum nature of light [19], and form a natural basis for other optical processes such as optical quantum key distribution, or ultrafast lithography.

2. Theory

An eigenmode travels through an optical system unchanged except for attenuation and a phase shift. If an image can be decomposed into its constituent eigenmodes, this

*Corresponding author. Email: allan.s.johnson@gmail.com

†Current address: School of Engineering & Physical Sciences, Heriot-Watt University, Edinburgh, UK.

attenuation and phase shift can be undone, and the original image can be reconstructed. In order to perform eigenmode super-resolution imaging, it is thus imperative that the eigenmodes of the system be known.

The propagation of an image through a linear optical system can be described in terms of a matrix multiplication mapping input fields to output fields. Finding the eigenmodes of the optical system is then equivalent to finding the eigenvectors of the system's characteristic matrix. To obtain the matrix, envision an arbitrary image Ψ as a superposition of complex fields that form a complete basis, i.e.

$$\Psi = \sum_n c_n \psi_n, \quad (1)$$

where the $\{\psi_n\}$ form a complete basis for the input and output complex fields and the $\{c_n\}$ are the complex coefficients that describe the test field in terms of the chosen basis. The output complex field can also be decomposed over the same orthogonal basis using an inner product, which is calculated by an overlap integral.

The overlap of two complex fields X and Y is given by

$$\langle X, Y \rangle = \int_D X Y^* d\sigma, \quad (2)$$

where D is the total area spanned by the detector and $d\sigma$ represents the differential area [24]. For pixelated detectors, this can also be written as a finite sum. The use of either continuous or discrete detectors will not affect any of the following discussion, except in that the space of possible modes is finite for finite detectors.

The complete transmission matrix T characterizing the optical system can then be found by sending the basis fields through the system sequentially and decomposing the output into those terms. The components of the final matrix are

$$T_{ij} = \langle S[\psi_i], \psi_j \rangle, \quad (3)$$

where $S[\psi_i]$ represents the output when the field ψ_i is incident on the optical system. Since the inner product requires the complex field at the output and not only the intensity, for an experimental implementation of this technique, a method of phase recovery is necessary. A versatile method of phase recovery is outlined in [25], relying on interference with a reference wave. The test mode characterization can be carried out through the use of spatial light modulators, where the reference wave can be directly written on the spatial light modulator along with the test mode [23]. Only recently has a full characterization of the transmission matrix become possible [25].

After determining the transmission matrix, we obtain its eigenvalues and eigenvectors using standard numerical techniques. The solutions to the eigenvalue equation $T\varphi_i = \lambda_i\varphi_i$, where φ_i is the i th eigenvector and λ_i its eigenvalue, represent eigenmodes in the original basis as

$$\Phi_i = \sum_{j=1}^N \varphi_{ij} \psi_j, \quad (4)$$

where N is the number of eigenmodes, φ_{ij} is the j th complex element of the eigenvector, and Φ_i is the eigenmode. See Figure 1 for some examples. Note that alternatively singular value decomposition could be utilized instead [17], in which case the output image must be decomposed over the right singular vectors and reconstructed over the left singular vectors, at an increased computational cost.

While our previous work has focused on the case of orthogonal eigenmodes, the existence of a normal transmission matrix is not guaranteed [26]. It is nevertheless possible to extend the technique to the case of non-orthogonal eigenmodes (singular vectors are automatically orthogonal). Consider the transmission of an arbitrary input field A , called the object, through the optical system. We express A in the eigenmode basis as

$$A = \sum_{i=1}^N a_i \Phi_i, \quad (5)$$

where A is the object, $\{\Phi_i\}$ are the eigenmodes, and $\{a_i\}$ are the coefficients that define the object. Since eigenvectors are linearly independent, this representation is unique. The transmission of this object through the optical system ($B = S[A]$) is

$$B = \sum_{i=1}^N \lambda_i a_i \Phi_i. \quad (6)$$

Each eigenmode Φ_i is attenuated and phase shifted by a potentially complex λ_i independently of the other components.

We want to determine the coefficients a_i from the output image. By considering the overlap of the output field B with the eigenmode Φ_j , the following linear equation is obtained:

$$\left\langle \sum_{i=1}^N \lambda_i a_i \Phi_i, \Phi_j \right\rangle = \langle B, \Phi_j \rangle. \quad (7)$$

In the case where the eigenmodes are orthogonal, as in an aberration-free, diffraction-limited $4f$ imaging system, $\langle \Phi_i, \Phi_j \rangle = \delta_{ij}$, and thus $\langle B, \Phi_j \rangle = \lambda_j a_j$ can be used to obtain the object coefficients directly, since λ_i and Φ_i are known. The $4f$ system, however, is a special case, and in general the eigenmodes of a system will not be orthogonal. In the non-orthogonal case it is instead necessary to consider the full system of equations obtained from the overlap of all eigenmodes with the complex field. For each eigenmode Φ_j the overlap equation can be expanded as:

$$\lambda_1 \varphi_{1j} \cdot \varphi_{j1} a_1 + \cdots + \lambda_N \varphi_{Nj} \cdot \varphi_{jN} a_N = b \cdot \varphi_j = \langle B, \Phi_j \rangle, \quad (8)$$

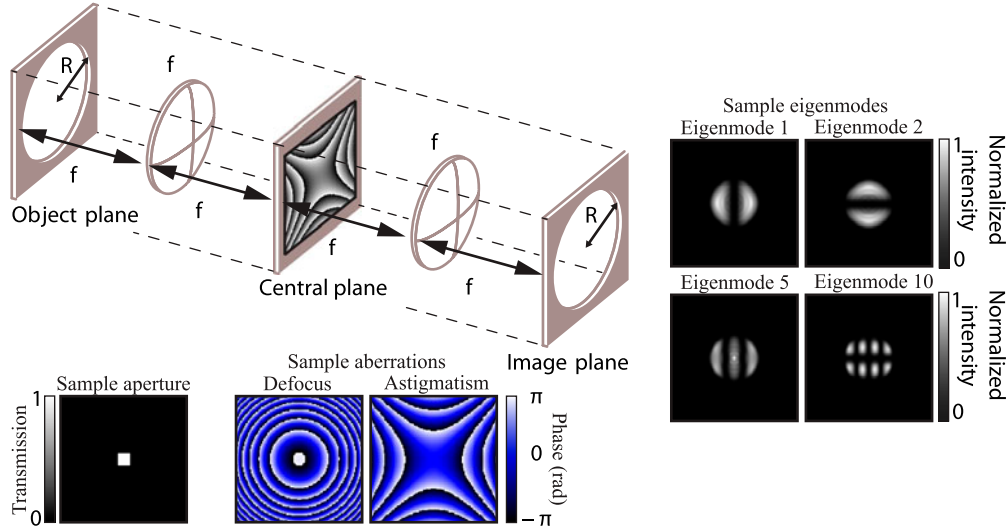


Figure 1. Schematic of the modelled $4f$ optical system and example eigenmodes. The object, central and image planes are separated by two lenses of focal length f , with the distance between each plane and adjacent lens also f . The object and image plane have apertures of radius R , and the central plane contains either a diffracting aperture or aberrations. Here, $f = 1$ m and $R = 2$ mm, while the light has a wavelength of 633 nm. Also shown are the first, second, fifth and tenth eigenmodes of the system in the presence of astigmatism of amplitude $z = 100$ rad across the simulation region. (The colour version of this figure is included in the online version of the journal.)

where b is the vector form of B in eigenmode basis. We can express the entire system of equations as a matrix multiplication:

$$\begin{bmatrix} \lambda_1 \varphi_1 \cdot \varphi_1 & \cdots & \lambda_N \varphi_N \cdot \varphi_1 \\ \vdots & \ddots & \vdots \\ \lambda_1 \varphi_1 \cdot \varphi_N & \cdots & \lambda_N \varphi_N \cdot \varphi_N \end{bmatrix} \begin{bmatrix} a_1 \\ \vdots \\ a_N \end{bmatrix} = \begin{bmatrix} b \cdot \varphi_1 \\ \vdots \\ b \cdot \varphi_N \end{bmatrix}. \quad (9)$$

This matrix multiplication can be more succinctly expressed as:

$$\Lambda A = \Gamma, \quad (10)$$

where Λ is the overlap of each eigenmode with each other eigenmode, weighted by its eigenvalue, A is the object in vector form and Γ is the overlap vector of the output with the eigenmodes. By discarding eigenvectors with vanishing eigenvalues, Λ is necessarily invertible (see Appendix 1), and the set of coefficients a_i can be found by solving Equation (12). At that the set of coefficients a_i define the object A , every image gives a unique reconstructed object.

To reduce the effect of noise on the reconstruction, we choose to include only those eigenvectors whose corresponding eigenvalues are above the noise threshold n_{thres} : $\lambda_k \geq n_{\text{thres}}$. The total number of eigenmodes used after thresholding is then given by N_{thres} , with $N_{\text{thres}} \leq N$. Thus we solve a modified form of Equation (12) in which we consider only the first N_{thres} modes, with Λ' an $N_{\text{thres}} \times N_{\text{thres}}$ matrix, and both A' and Γ' as column vectors of length N_{thres} . Once this solution is obtained, it is simple to build a reconstruction of the original image using Equation (5) within the reduced space spanned by the N_{thres} eigenmodes. Note this necessarily enforces the condition of

non-vanishing eigenvalues, and ensures invertibility. In the case of pixelated detectors, there exists a hard cut-off of D independent vectors, where D is the number of pixels, but the results are otherwise unchanged.

The effect of discarding eigenmodes with transmission below the noise threshold has been discussed in great detail elsewhere; we refer the interested reader to [16,17,27–29] for detailed discussions on the impact of this step on resolution. As we will show, in practice this step results in increased resolution for a variety of typical images.

3. Numerical methods

To demonstrate the technique outlined above, we perform simulations of an optical system containing diffracting apertures or aberrations. The optical system we consider is a $4f$ system with circular apertures in the object and image planes and diffracting apertures or aberrations in the central plane; see Figure 1. Unlike previous work, the eigenmodes of these systems are not known analytically. Diffraction is controlled by changing the size or shape of the diffracting aperture, while aberrations are modelled by the Zernike polynomials Z_2^0 , Z_2^2 , and Z_3^{-3} by controlling the amplitude of the polynomial z [30].

We characterize the optical system using the Laguerre–Gaussian (LG) basis $\{\psi_n\} = \{\text{LG}_{\ell p}\}$ [31]. In our simulations, a total of 121 LG modes are used to characterize the optical systems, with indices $-5 \leq \ell \leq 5$ and $0 \leq p \leq 10$. The basis functions must be chosen in order to adequately probe all degrees of freedom of the optical system. In a few special cases the degrees of freedom are analytically

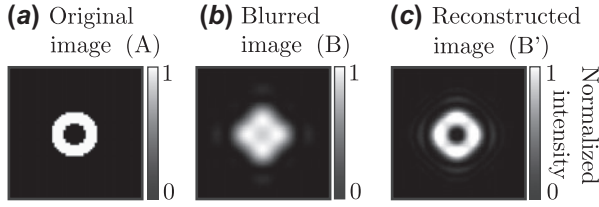


Figure 2. Numerical super-resolution results in the presence of a diffracting square aperture of size 1 mm by 1 mm. 56 eigenmodes are used in each reconstruction. (a) The original image propagated through the $4f$ system with a diffracting square aperture. (b) The output image. (c) The super-resolved image.

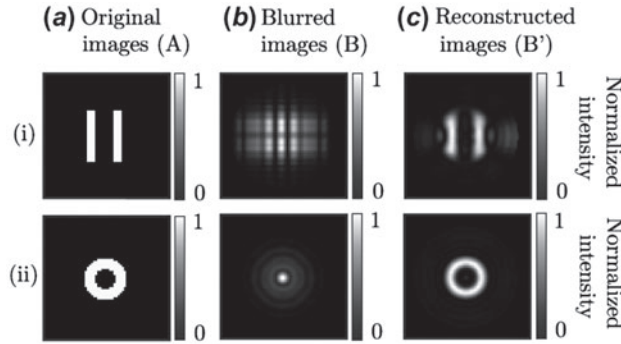


Figure 3. Numerical eigenmode imaging results in the presence of defocus of amplitude $z = 48$ rad across the simulation region. 59 eigenmodes are used in each reconstruction. (a) The original images propagated through the aberrated system. (b) The output images. (c) The reconstructed images.

known and appropriate basis functions can be chosen; in general, choosing a basis which shares symmetry characteristics with the system and using all modes with significant transmission is sufficient. The closer the initial guess set of test modes is to the eigenmodes, the fewer modes that need to be tested. In order to obtain the same results as with 121 LG modes, approximately 900 plane waves have to be used for the systems here.

Once the system is characterized, an image is propagated through the optical systems and the object is reconstructed. The super-resolution factor, defined as

$$S_r = \left| \frac{\langle B', A \rangle}{\langle B, A \rangle} \right|^2 - 1, \quad (11)$$

where B' is the reconstructed object, is then computed. The super-resolution factor gives a dimensionless measure of the image enhancement. When $S_r > 0$, it indicates that the image has been super-resolved. Though super-resolution strictly applies to sub-diffraction imaging, we will also use S_r to quantify improvements in systems with aberrations, and thus refer to reconstructed images for any system with $S_r > 0$ as being super-resolved.

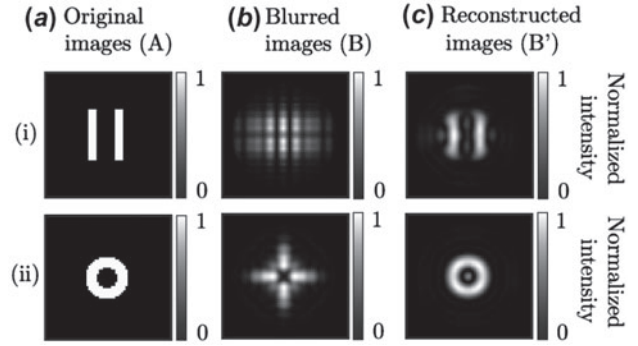


Figure 4. Numerical eigenmode imaging results in the presence of astigmatism of amplitude $z = 100$ rad across the simulation region. 49 eigenmodes are used in each reconstruction. (a) The original images propagated through the aberrated system. (b) The output images. (c) The reconstructed images.

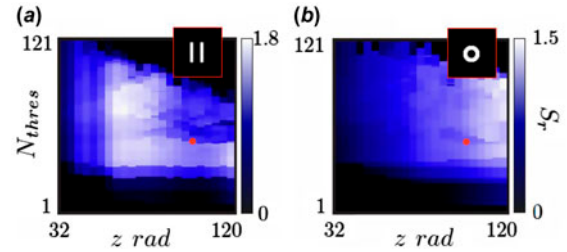


Figure 5. Super-resolution factors S_r for reconstructed images (object shown as inset) as a function of amplitude of astigmatism z and the number of eigenmodes used to reconstruct, N_{thres} . The red circle indicates the images in Figure 4 (colour online). (The colour version of this figure is included in the online version of the journal).

4. Results

Figure 2 shows super-resolution in the case of a diffracting square aperture of size 1 mm \times 1 mm. The original image is shown in column (a), the diffracted output in column (b) and the reconstructed image in column (c). This result is obtained using 56 eigenmodes to perform reconstruction. As reconstructions contain some obvious low-level noise features, images are additionally thresholded above this level (approximately 10% of total intensity). By comparing the images in columns (b) and (c), clear and dramatic increases in image quality can be seen. The super-resolution factor is found to be $S_r = 0.32$. This improvement is clearly significant enough to distinguish the object as a ring from the super-resolved image, whereas such a clear conclusion is impossible from the diffracted image. The eigenmodes are found not to be orthogonal in this system, and thus this successful reconstruction relies upon both Equation (12), and the successful determination of the system's eigenmodes.

Figure 3 shows results for a sample aberration, defocus of magnitude $z = 48$ rad across the simulation region. The original image is shown in column (a), the blurred output in column (b) and the reconstructed image in column (c).

These results are obtained using 59 eigenmodes to perform reconstruction. For these images, $S_r = 1.7$ and $S_r = 1.2$ respectively. While some noise is introduced by the reconstruction procedure, the main features of each image, which are completely obscured in the blurred output, are restored.

Figure 4 shows results for astigmatism of magnitude $z = 100$ rad across the simulation region. The original image is shown in column (a), the blurred output in column (b) and the reconstructed image in column (c). These results are obtained using 49 eigenmodes to perform reconstruction. Once again dramatic increases in image quality can be seen. For these images, $S_r = 1.3$ and $S_r = 1.0$ respectively.

Figure 5 shows S_r for two images (inset) as a function of the number of modes used to reconstruct and the magnitude of astigmatism across the simulation region. As can be seen, for each level of aberration there exists an optimal number of modes to use in order to obtain the best super-resolution factor. Since for different images the overlap with each eigenmode will change, the number of eigenmodes used to obtain the optimum super-resolution factor will vary depending on the image. However an operating point N_{thres} can always be chosen such that both images are super-resolved. Thus the technique of eigenmode super-resolution is neither target nor system specific, and while results will show varying degrees of improvement, improvement should always be possible.

The freedom of choice in N_{thres} necessarily introduces a degree of freedom in the reconstructed image. There is therefore a trade-off of images reconstructed with too few modes which are blurred and exhibit artefacts, and images reconstructed with too many modes which are vulnerable to noise amplification. Thus the limits to the quality of a reconstructed image are set by the noise and the eigenmodes of the system, meaning any system would require calibration prior to use in order to determine an optimal operating point.

Different sources of noise will affect the ability to perform an accurate reconstruction in differing ways. For example, one can be subject to noise in the characterization stage or in the object transmission. The characterization stage determines the eigenmodes and eigenvalues that are used in the reconstruction, and it is crucial to calculate these accurately. While a full analysis of the noise performance is beyond the scope of this work, noise introduced at the characterization stage is found to have a more significant impact than noise introduced in the object transmission.

In a system purely limited by diffraction, the eigenmodes are sufficient to compose any image, making noise the only limit to super-resolution [18]. Moving to the reduced eigenmode basis in this case yields superior results, despite the apparent discarding of information. If an eigenmode has transmission below the noise threshold, the information in this mode is already lost to noise and cannot be recovered by this technique (or indeed any other). Reconstructing the projection of the image into the imaging system's viable space offers, in practise, a sufficiently improved image to enable

recognition of most features in the original image. In other systems, such as a multi-mode fibre, the fundamental limits are more pronounced, but eigenmode super-resolution may still yield dramatic improvement.

5. Conclusions

In summary, we investigate eigenmode super-resolution in the case of an arbitrary optical system. We show how to find the eigenmodes of such a system and use them for super-resolution in the case of non-orthogonal eigenmodes. We furthermore numerically simulate and apply the technique to various systems, and we show significant improvement is possible independent of the object. Future work will focus on experimentally demonstrating eigenmode imaging in systems where the eigenmodes are not known analytically, and examining the quantum limits to resolution in such systems. Eigenmodes will also enable imaging through turbulence, quantum key distribution through optical fibre, and form an optimal basis for lithography.

Acknowledgements

We thank Kevin Church for assistance with the properties of invertible matrices.

Funding

This work was supported by the Canada Excellence Research Chairs (CERC) Program. In addition, RWB acknowledges support from the DARPA InPho program.

References

- [1] Abbe, E. *Arch. Mikrosk. Anat.* **1873**, 9, 413–418.
- [2] Harris, J.L. *J. Opt. Soc. Am.* **1964**, 54 (7), 931–933.
- [3] Lukosz, W. *J. Opt. Soc. Am.* **1966**, 56 (11), 1463–1471.
- [4] Pendry, J. *Phys. Rev. Lett.* **2000**, 85, 3966–3969.
- [5] Smith, D.R. *Science (New York, N.Y.)* **2005**, 308 (5721), 502–503.
- [6] Fang, N. *Science* **2005**, 308 (5721), 534–537.
- [7] Liu, Z.; Lee, H.; Xiong, Y.; Sun, C.; Zhang, X. *Science (New York, N.Y.)* **2007**, 315 (5819), 1686–1687.
- [8] Hell, S.W.; Wichmann, J. *Opt. Lett.* **1994**, 19, 780–782.
- [9] Westphal, V.; Rizzoli, S.O.; Lauterbach, M.A.; Kamin, D.; Jahn, R.; Hell, S.W. *Science* **2008**, 320 (5873), 246–249.
- [10] Rittweger, E.; Han, K.Y.; Irvine, S.E.; Eggeling, C.; Hell, S.W. *Nat. Photonics* **2009**, 3, 144–147.
- [11] Rogers, E.T.F.; Lindberg, J.; Roy, T.; Savo, S.; Chad, J.E.; Dennis, M.R.; Zheludev, N.I. *Nat. Mater.* **2012**, 11 (5), 432–435.
- [12] Gazit, S.; Szameit, A.; Eldar, Y.C.; Segev, M. *Opt. Express* **2009**, 17 (26), 23920–23946.
- [13] Shechtman, Y.; Eldar, Y.C.; Szameit, A.; Segev, M. *Opt. Express* **2011**, 19 (16), 14807–14822.
- [14] Shin, H.; Chan, K.W.C.; Chang, H.J.; Boyd, R.W. *Phys. Rev. Lett.* **2011**, 107, 083603.
- [15] Giovannetti, V.; Lloyd, S.; Maccone, L.; Shapiro, J.H. *Phys. Rev. A* **2009**, 79, 013827.
- [16] Francia, G.D. *J. Opt. Soc. Am.* **1969**, 59 (7), 799–804.
- [17] Bertero, M.; Pike, E. *J. Opt. Soc. Am.* **1982**, 29 (6), 727–746.

- [18] Kolobov, M.I.; Fabre, C. *Phys. Rev. Lett.* **2000**, *85*, 3789–3792.
- [19] Beskrovny, V.N.; Kolobov, M.I. *Phys. Rev. A* **2008**, *78*, 043824.
- [20] Fish, D.A.; Grochmalicki, J.; Pike, E.R. *J. Opt. Soc. Am. A* **1996**, *13*, (3), 464–469.
- [21] Pike, R.; Chana, D.; Neocleous, P.; Jiang, S. *Opt. Imaging Microsc.* **2003**, *87*, 87–110.
- [22] Akduman, I.; Brand, U.; Grochmalicki, J.; Hester, G. *J. Opt. Soc. Am.* **1998**, *15* (9), 2275–2287.
- [23] Piché, K.; Leach, J.; Johnson, A.S.; Salvail, J.Z.; Kolobov, M.I.; Boyd, R.W. *Opt. Express* **2012**, *20* (24), 26424–26433.
- [24] De Luca, A.C.; Kosmeier, S.; Dholakia, K.; Mazilu, M. *Phys. Rev. A* **2011**, *84*, 021803.
- [25] Popoff, S.M.; Lerosey, G.; Carminati, R.; Fink, M.; Boccarda, A.C.; Gigan, S. *Phys. Rev. Lett.* **2011**, *104* (10), 100601.
- [26] Siegman, A. *Opt. Commun.* **1979**, *31* (3), 369–373.
- [27] Rushforth, C.; Harris, R. *J. Opt. Soc. Am.* **1968**, *58* (4), 539–544.
- [28] Beskrovny, V.N.; Kolobov, M.I. *Opt. Commun.* **2006**, *264* (1), 9–12.
- [29] Beskrovny, V.; Kolobov, M. *Phys. Rev. A* **2008**, *78* (4), 043824.
- [30] Born, M.; Wolf, E. *Principles of Optics: Electromagnetic Theory of Propagation, Interference, and Diffraction of Light*; 7th ed. (Expanded); Cambridge University Press: Cambridge, UK, 1999.
- [31] Allen, L.; Beijersbergen, M.W.; Spreeuw, R.J.C.; Woerdman, J.P. *Phys. Rev. A* **1992**, *45*, 8185–8189.

Appendix 1. Supplementary information

In a system with non-orthogonal eigenmodes, in order for reconstruction to give a unique solution, the equation

$$\Lambda A = \Gamma, \quad (12)$$

must have a unique solution for A , the object, given any image Γ . This condition is satisfied if the matrix

$$\Lambda = \begin{bmatrix} \lambda_1 \varphi_1 \cdot \varphi_1 & \cdots & \lambda_N \varphi_N \cdot \varphi_1 \\ \vdots & \ddots & \vdots \\ \lambda_1 \varphi_1 \cdot \varphi_N & \cdots & \lambda_N \varphi_N \cdot \varphi_N \end{bmatrix} \quad (13)$$

is invertible. We will now show that provided only non-vanishing eigenmodes are considered, which is to say eigenmodes with non-vanishing eigenvalues, this condition is satisfied. This condition is automatically satisfied by the reduced form of Λ in the text.

We start by noting that a square matrix is invertible if it has full rank. It suffices to show then that

$$\text{rank } \Lambda = N \quad (14)$$

in order to prove the matrix is invertible.

The rank of a matrix is invariant under several important transformations. Primarily, as the rank of matrix is equivalent to the dimension of its column space, the rank is invariant under column operations (scalar multiplication and addition of columns). This allows us to state that

$$\text{rank } \Lambda = \text{rank} \begin{bmatrix} \varphi_1 \cdot \varphi_1 & \cdots & \varphi_N \cdot \varphi_1 \\ \vdots & \ddots & \vdots \\ \varphi_1 \cdot \varphi_N & \cdots & \varphi_N \cdot \varphi_N \end{bmatrix}, \quad (15)$$

provided that $\forall i, \lambda_i \neq 0$.

Furthermore, for any matrix M ,

$$\text{rank } M = \text{rank } M^* = \text{rank } M^T, \quad (16)$$

where M^* denotes the scalar complex conjugate and M^T the transpose. We can then consider the rank of the conjugate matrix from Equation (15).

The conjugated matrix can be written as the product of two simpler matrices,

$$\begin{bmatrix} \varphi_1 \cdot \varphi_1 & \cdots & \varphi_1 \cdot \varphi_N \\ \vdots & \ddots & \vdots \\ \varphi_N \cdot \varphi_1 & \cdots & \varphi_N \cdot \varphi_N \end{bmatrix} = [\varphi_1 \cdots \varphi_N]^T [\varphi_1 \cdots \varphi_N], \quad (17)$$

which are expressed in block column notation. We can then use Sylvester's rank inequality to state that

$$\text{rank } \Lambda \geq \text{rank} [\varphi_1 \cdots \varphi_N]^T + \text{rank} [\varphi_1 \cdots \varphi_N] - N \quad (18)$$

$$\geq 2 \text{rank} [\varphi_1 \cdots \varphi_N] - N, \quad (19)$$

where we have used Equation (16) to remove the transpose.

Since the eigenvectors are by definition linearly independent, the matrix $[\varphi_1 \cdots \varphi_N]$ is composed entirely of linearly independent columns. Thus its column space has dimension N , and accordingly rank N . Substituting this into Equation (19),

$$\text{rank } \Lambda \geq 2N - N, \quad (20)$$

$$\text{rank } \Lambda = N, \quad (21)$$

as the rank of a matrix cannot exceed its dimension. Thus Λ has full rank and is invertible, guaranteeing the existence of a solution to Equation (12) and that a unique object will be obtained for every image.